

# Two-Layer Reinforcement Learning-Assisted Joint Beamforming and Trajectory Optimization for Multi-UAV Downlink Communications

Ruiqi Wang, Esraa M. Ghourab, *Senior Member, IEEE*, Omar Alhussein, *Senior Member, IEEE*, Yuzhi Yang, *Member, IEEE*, Yuhang Sheng, Jing Ren, *Member, IEEE*, Shizhong Xu, *Member, IEEE*, and Sami Muhaidat, *Senior Member, IEEE*

**Abstract**—Unmanned aerial vehicles (UAVs) are pivotal for future 6G non-terrestrial networks, yet their high mobility creates a complex coupled optimization problem for beamforming and trajectory design. Existing numerical methods suffer from prohibitive latency, while standard deep learning often ignores dynamic interference topology, limiting scalability. To address these issues, this paper proposes a hierarchically decoupled framework synergizing graph neural networks (GNNs) with multi-agent reinforcement learning. Specifically, on the short timescale, we develop a topology-aware GNN beamformer by incorporating GraphNorm. By modeling the dynamic UAV-user association as a time-varying heterogeneous graph, this method explicitly extracts interference patterns to achieve sub-millisecond inference. On the long timescale, trajectory planning is modeled as a decentralized partially observable Markov decision process and solved via the multi-agent proximal policy optimization algorithm under the centralized training with decentralized execution paradigm, facilitating cooperative behaviors. Extensive simulation results demonstrate that the proposed framework significantly outperforms state-of-the-art optimization heuristics and deep learning baselines in terms of system sum rate, convergence speed, and generalization capability.

**Index Terms**—Unmanned aerial vehicle, beamforming design, trajectory optimization, graph neural network, multi-agent reinforcement learning.

## I. INTRODUCTION

Unmanned aerial vehicles (UAVs) have emerged as a pivotal component of future 6G non-terrestrial, offering flexible 3D deployment for on-demand coverage [1]. However, the UAVs' spatial-temporal trajectories dictate the channel topology, which brings a trade-off between the UAV moving constraints and communication performance. Moreover, the limited beamforming capabilities conversely constrain the flight paths to mitigate interference [2]. This intricate interdependence creates a complex control problem, further exacerbated in multi-UAV scenarios by the imperatives of cooperative interference management and collision avoidance.

To tackle this problem, existing literature has traditionally resorted to iterative numerical optimization [2]. However, it suffers from prohibitive computational latency due to the computational complexity, making it inadequate for real-time decision-making. Meanwhile, reinforcement learning (RL)-based approaches offer faster inference on such complex optimization problems, while facing two main challenges. First, standard end-to-end architectures are typically structure-agnostic, making it hard to capture the intrinsic graph topology

of user association. There is also an inherent timescale mismatch between small-scale fading channels fluctuating on the order of milliseconds and UAV mechanical mobility evolving over seconds. Thus, treating these distinct dynamics as a monolithic synchronous process leads to an intractable hybrid action space. To address this, we propose a hierarchically decoupled framework that separates the problem into an inner-loop for instantaneous beamforming and an outer-loop for long-term trajectory planning.

For the inner-loop beamforming, the multi-UAV environment is characterized by dynamic graph-structured topologies, which can be captured by a graph neural network (GNN). Distinguished from conventional neural networks that require fixed-dimensional inputs, GNNs leverage permutation invariance and parameter sharing to explicitly capture dynamic and irregular interference topologies [3] [4]. Building upon this paradigm, we propose a topology-aware GNN model to directly conduct optimal beamforming by real-time channel state information (CSI). Specifically, we model the dynamic UAV-user system as a time-varying heterogeneous graph. Leveraging a heterogeneous message passing mechanism, this design efficiently captures the coupled interference patterns.

For the outer-loop trajectory planning, the problem represents a complex sequential decision-making process plagued by non-stationarity induced by the simultaneous evolution of multiple agents' policies. Multi-agent reinforcement learning (MARL) under the centralized training with decentralized execution (CTDE) paradigm is inherently suitable for such cooperative tasks [5] [6]. Within this framework, we employ the multi-agent proximal policy optimization (MAPPO) algorithm to ensure superior stability in stochastic policy optimization [7]. However, the direct deployment of standard MAPPO in this specific scenario faces challenges, particularly stemming from the sparse feedback inherent in long-term trajectory planning and the training instability caused by asynchronous mission completions, where different UAVs reach their destinations at varying time steps due to diverse flight distances. To address these challenges, we enhance the algorithm by designing a novel reachability-aware reward mechanism coupled with an arrival masking scheme. This dual-mechanism provides dense, step-wise supervision on flight feasibility while effectively filtering out invalid gradients from completed agents, thereby complementing the global value estimation. Consequently, our tailored approach enables agents to learn sophisticated

cooperative behaviors based on the reward feedback from the inner-loop beamformer.

Generally, we integrate the proposed topology-aware GNN and the feasibility-enhanced MAPPO into a cohesive closed-loop system in this paper. This synergistic design enables the inner-loop beamformer to provide accurate, instantaneous reward feedback, thereby guiding the outer-loop agents to learn globally optimal strategies that balance flight safety with communication quality. The main contributions of this paper are summarized as follows:

- We propose a timescale-separated framework that decomposes the joint optimization into instantaneous beamforming and continuous trajectory planning, effectively resolving their misalignment in timescales.
- We design a topology-aware GNN model to solve the real-time beamforming problem, which enables scalable interference management across variable network densities.
- We propose to solve the multi-UAV path planning problem using MAPPO under the CTDE paradigm. To tackle the challenges of sparse feedback and asynchronous termination, we introduce a novel reachability-aware reward mechanism coupled with an arrival masking scheme, explicitly facilitating stable and efficient long-horizon cooperation.
- Extensive simulations demonstrate that our framework achieves sub-millisecond inference latency and outperforms strong baselines. Notably, it exhibits strong generalization capabilities in scenarios with diverse user densities and topologies.

The remainder of this paper is organized as follows: The related works are summarized in Section II. The system model and problem formulation are introduced in Section III. The GNN-based beamforming is proposed in Section IV and the MAPPO-based multi-UAV trajectory planning is introduced in Section V. Simulation results are discussed in Section VI. Finally, the conclusion and future work of this paper are summarized in Section VII.

## II. RELATED WORK

Research on the joint beamforming and trajectory optimization design for UAV-assisted wireless communications has undergone a gradual evolution, progressing from conventional optimization-based methods to learning-based methods, and more recently to graph-based methods.

### A. Optimization-Based Frameworks

Conventional mathematical optimization techniques have been extensively employed to address the coupled design of UAV trajectory and communication resources.

Fundamental studies typically formulate these designs as non-convex optimization problems, solving them via iterative algorithms such as block coordinate descent and successive convex approximation (SCA) [8]. To exploit the high directionality of millimeter-wave (mmWave) channels, these frameworks were extended by integrating heuristic algorithms (e.g., artificial bee colony) [9] or matching theory [10] to handle beamforming

and user clustering. Furthermore, energy-efficient designs have been explored in wireless power transfer scenarios by handling non-linear energy harvesting models via SCA [11]. Recent advancements have incorporated reconfigurable intelligent surfaces to reconfigure the propagation environment. Studies in this domain [12]–[14] generally decompose the problem into active beamforming, passive beamforming, and trajectory optimization sub-problems, solving them alternately using techniques like fractional programming. More recently, optimization-based frameworks have been applied to emerging complex scenarios with stringent coupling constraints, including integrated sensing and communication [15]–[17], covert communications [18], [19], and satellite-terrestrial coexistence [20]. These works tackle challenges such as interference management, robustness against CSI uncertainty, and multi-objective coupling by utilizing advanced methods like semidefinite relaxation, S-Procedure, and model predictive control.

Despite their theoretical rigor, optimization-based methods incur prohibitive computational latency and scale poorly. Furthermore, their reliance on static snapshots often fails to capture the instantaneous topological changes inherent in multi-UAV flight, motivating our scalable, real-time learning-based framework. These limitations underscore the need for a learning-based framework that can efficiently facilitate scalable, real-time cooperative decision-making.

### B. Learning-Based Frameworks

To overcome the high computational complexity and limited real-time adaptability of conventional optimization methods, RL has been widely adopted to learn decision-making policies directly from environmental interactions.

Initial studies focused on single-UAV scenarios, utilizing continuous control algorithms like deep Q-network [21] [22] and deep deterministic policy gradient [22] to manage coupled trajectory and phase-shift designs in dynamic environments. Beyond pure RL, supervised learning techniques such as recurrent neural networks have also been employed to predict beam alignment in high-mobility contexts [23]. As network scale increases, research has shifted towards MARL to handle collaborative tasks [5]. Liu et al. [6] developed an improved heterogeneous-agent trust region policy optimization algorithm to synchronize phases among multiple UAVs for collaborative beamforming, while Chiang et al. [24] combined Q-learning with optimization for mmWave beam tracking. Furthermore, to address conflicting performance metrics in complex heterogeneous networks, multi-objective DRL algorithms have been introduced to balance throughput and energy efficiency [25]. Recent advancements have further integrated emerging paradigms to enhance privacy and generalization. For instance, federated DRL was proposed to optimize space-air-ground networks while preserving data privacy [26]. Most recently, large language models have been utilized to guide DRL exploration, significantly improving sample efficiency in unseen environments [27].

While efficient, standard learning-based methods treat the wireless environment as a simple Euclidean space, ignoring the inherent graph-structured interference topology. This structural

agnosticism leads to poor generalization across varying network scales, necessitating a shift towards graph-based paradigms for scalable, topology-aware optimization.

### C. Graph-Based Frameworks

Motivated by the inherent graph-structured nature of wireless networks, GNNs have been introduced to explicitly capture node connectivity and interference coupling.

Early works applied GNNs primarily for snapshot-based resource allocation. For instance, Li et al. [28] utilized GNN to optimize link scheduling in multi-UAV D2D networks by learning interference topologies. To capture high-order interference beyond pairwise connections, Zhao et al. [29] proposed a hypergraph-based learning framework for beamforming in UAV-assisted Internet of things systems. Similarly, Wang et al. [30] employed GNNs to optimize the static 3D placement and resource allocation for UAV access points by extracting spatial user distribution features. More recently, hybrid frameworks combining GNNs with DRL have emerged to address sequential decision-making problems. Pan et al. [31] integrated GNNs into the QMIX algorithm to enhance state representation under partial observability for age of information management. Extending this paradigm to continuous mobility control, recent studies have begun to integrate graph representation learning directly with UAV trajectory planning. Specifically, Tang et al. [3], and Wang et al. [4] both combined GNN with the RL algorithm to develop a hybrid framework to solve the joint optimization problem of beamforming and trajectory planning, where GNNs extract topological features for beamforming prediction and the RL algorithm for trajectory optimization.

However, these existing GNN-RL hybrid frameworks [3] [4] generally focus on single-UAV scenarios with a fixed set of served users throughout the mission. In such setups, the graph scale remains static, and the challenge of dynamic user association is absent. In contrast, this paper investigates a multi-UAV network where user association and interference topology change dynamically due to the UAVs' mobility and limited coverage. We propose a dynamic heterogeneous graph modeling approach integrated with MAPPO to handle the time-varying set of served users and the complex multi-UAV cooperative trajectory planning, ensuring scalable and cooperative decision-making in highly dynamic environments.

## III. SYSTEM MODEL AND PROBLEM FORMULATION

As illustrated in Fig. 1, we investigate a multi-UAV multi-user downlink communication network, where a set of  $N$  rotary-wing UAVs, denoted by  $\mathcal{N} = \{1, \dots, N\}$ , are dispatched to serve  $K$  randomly distributed ground users, denoted by  $\mathcal{K} = \{1, \dots, K\}$ . Each UAV  $n \in \mathcal{N}$  is equipped with a uniform linear array (ULA) of  $L$  antennas, whereas each user is equipped with a single omnidirectional antenna. We assume that all UAVs fly at a fixed operational altitude  $H$  with a constant speed  $V$ . The system operation timeline is discretized into equal-length time slots indexed by  $t \in \mathcal{T} = \{1, \dots, T\}$ , where the duration of each slot is  $\delta_t$ . Without loss of generality, we adopt a 3D Cartesian coordinate system. The location of

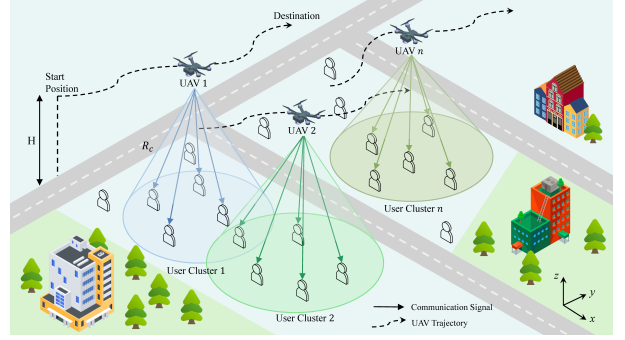


Fig. 1: System model

user  $k$  is fixed at  $\mathbf{l}_k^U = [x_k^u, y_k^u, 0]^T$ . Meanwhile, the time-varying position of UAV  $n$  at time slot  $t$  is denoted by  $\mathbf{l}_n^A[t] = [x_n^a[t], y_n^a[t], H]^T$ . For the trajectory planning task, each UAV  $n$  is required to travel from a predefined starting point  $\mathbf{l}_n^S = [x_n^s, y_n^s, H]^T$  to a destination point  $\mathbf{l}_n^D = [x_n^d, y_n^d, H]^T$  within the maximum mission duration  $T_{\max}$ , while simultaneously providing downlink data transmission to the served users.

### A. Dynamic User Association and UAV Mobility

To guarantee reliable link quality, we assume that each UAV has a limited communication coverage radius, denoted by  $R_c$ . A user  $k$  is considered serviceable by UAV  $n$  only if it resides within the coverage region, satisfying the geometric constraint  $\|\mathbf{l}_n^A[t] - \mathbf{l}_k^U\| \leq R_c$ . To handle the overlapping coverage areas, we adopt a nearest-neighbor association protocol. Specifically, at any time slot  $t$ , a user is associated with the spatially closest UAV among those covering it. Consequently, the user set served by UAV  $n$  at time slot  $t$ , denoted by  $\mathcal{K}_n[t]$ , is referred to as a user cluster:

$$\mathcal{K}_n[t] = \left\{ k \in \mathcal{K}_n[t] \mid \|\mathbf{l}_n^A[t] - \mathbf{l}_k^U\| \leq R_c, \right. \\ \left. n = \arg \min_{j \in \mathcal{N}} \|\mathbf{l}_j^A[t] - \mathbf{l}_k^U\| \right\}. \quad (1)$$

Furthermore, to eliminate severe inter-cluster interference among neighboring UAVs, we assume that the total system bandwidth is orthogonally allocated to different UAVs (e.g., via frequency division multiple access), following the standard frequency reuse principle widely adopted in cellular networks [32]. Under this assumption, the multi-UAV network is decoupled into  $N$  locally independent downlink subsystems [33]. Thus, the signal quality of each user is solely determined by the channel gain from its serving UAV and the intra-cluster interference caused by other users within the same cluster  $\mathcal{K}_n[t]$ .

The mobility of UAVs is modeled as a discrete-time decision-making process. At each time slot  $t$ , UAV  $n$  executes a movement action  $\mathbf{a}_n[t]$ , which dictates its displacement for the subsequent time slot. To ensure the physical feasibility and safety of the flight trajectories, the following constraints are imposed:

- **Collision Avoidance:** To prevent aerial accidents, a minimum safety distance  $D_{\min}$  must be strictly main-

tained between any pair of UAVs throughout the mission duration:

$$\|\mathbf{l}_n^A[t] - \mathbf{l}_m^A[t]\|^2 \geq D_{\min}^2, \quad \forall n \neq m, \forall t \in \mathcal{T}. \quad (2)$$

- **Flight Range Limits:** To ensure the UAVs operate within the service area, the horizontal position of each UAV  $n$  is strictly bounded by the predefined rectangular region  $[x_{\min}, x_{\max}] \times [y_{\min}, y_{\max}]$ :

$$x_{\min} \leq x_n^u[t] \leq x_{\max}, \quad \forall n \in \mathcal{N}, \forall t \in \mathcal{T}, \quad (3)$$

$$y_{\min} \leq y_n^u[t] \leq y_{\max}, \quad \forall n \in \mathcal{N}, \forall t \in \mathcal{T}. \quad (4)$$

- **Mission Duration Constraint:** Due to on-board battery limitations, each UAV  $n$  is required to arrive at its destination  $\mathbf{l}_n^D$  within a maximum allowable flight duration  $T_{\max}$ . Let  $T$  denote the actual system operation time, defined as the maximum completion time among all UAVs. This imposes the constraint:

$$T \triangleq \max_{n \in \mathcal{N}} T_n \leq T_{\max}. \quad (5)$$

### B. Channel Model and Signal Transmission

Given the dynamic mobility of UAVs, the air-to-ground (A2G) channels exhibit strong time-varying characteristics. We adopt a Line-of-Sight (LoS) dominated channel model, which is widely used for UAV communications in high-altitude scenarios [8] [9] [13]. At time slot  $t$ , the channel vector  $\mathbf{h}_{n,k}[t] \in \mathbb{C}^{L \times 1}$  between UAV  $n$  and user  $k$  is modeled as:

$$\mathbf{h}_{n,k}[t] = \sqrt{\beta_{n,k}[t]} \mathbf{a}(\theta_{n,k}[t]), \quad (6)$$

where  $\beta_{n,k}[t] = \beta_0 (d_0/d_{n,k}[t])^{-2}$  represents the large-scale path loss. Here,  $d_{n,k}[t] = \|\mathbf{l}_n^A[t] - \mathbf{l}_k^U\|$  denotes the instantaneous distance,  $\beta_0$  is the channel power gain at the reference distance  $d_0$  m. Furthermore,  $\mathbf{a}(\theta_{n,k}[t])$  denotes the array steering vector. Assuming each UAV is equipped with a ULA with antenna spacing  $d_a$ , the steering vector is given by:

$$\mathbf{a}(\theta_{n,k}[t]) = \left[ 1, e^{j2\pi \frac{d_a}{\lambda} \cos \theta_{n,k}[t]}, \dots, e^{j2\pi \frac{d_a}{\lambda} (L-1) \cos \theta_{n,k}[t]} \right]^T, \quad (7)$$

where  $\lambda$  is the carrier wavelength, and  $\theta_{n,k}[t]$  represents the elevation angle of departure (AoD), calculated as  $\theta_{n,k}[t] = \arccos(H/d_{n,k}[t])$ .

To support downlink transmission, UAV  $n$  employs a linear precoding vector  $\mathbf{w}_{n,k}[t] \in \mathbb{C}^{L \times 1}$  for each associated user  $k \in \mathcal{K}_n[t]$ , which is controlled by the beamforming algorithm. The transmitted signal  $\mathbf{x}_n[t]$  is the superposition of data symbols intended for its serving cluster:

$$\mathbf{x}_n[t] = \sum_{k \in \mathcal{K}_n[t]} \mathbf{w}_{n,k}[t] s_{n,k}[t], \quad (8)$$

where  $s_{n,k}[t] \sim \mathcal{CN}(0, 1)$  is the normalized data symbol. The transmit power of each UAV is constrained by a maximum budget  $P_{\max}$ :

$$\sum_{k \in \mathcal{K}_n[t]} \|\mathbf{w}_{n,k}[t]\|^2 \leq P_{\max}, \quad \forall n \in \mathcal{N}. \quad (9)$$

The received signal at user  $k$  (served by UAV  $n$ ) comprises the desired signal, the intra-cluster interference from other users served by the same UAV, and the additive noise:

$$y_k[t] = \underbrace{\mathbf{h}_{n,k}^H[t] \mathbf{w}_{n,k}[t] s_{n,k}[t]}_{\text{Desired Signal}} + \underbrace{\sum_{j \in \mathcal{K}_n[t], j \neq k} \mathbf{h}_{n,k}^H[t] \mathbf{w}_{n,j}[t] s_{n,j}[t] + z_k[t]}_{\text{Intra-cluster Interference}}, \quad (10)$$

where  $z_k[t] \sim \mathcal{CN}(0, \sigma_0^2)$  denotes the Additive White Gaussian Noise (AWGN). The achievable Signal-to-Interference and Noise Ratio (SINR) is given by:

$$\gamma_k[t] = \frac{|\mathbf{h}_{n,k}^H[t] \mathbf{w}_{n,k}[t]|^2}{\sum_{j \in \mathcal{K}_n[t], j \neq k} |\mathbf{h}_{n,k}^H[t] \mathbf{w}_{n,j}[t]|^2 + \sigma_0^2}. \quad (11)$$

Accordingly, the achievable data rate of user  $k$  at time slot  $t$  is given by:

$$R_k[t] = \log_2(1 + \gamma_k[t]). \quad (12)$$

### C. Problem Formulation

Our primary objective is to maximize the long-term average sum rate  $\bar{R}$  by jointly optimizing the active beamforming vectors  $\mathcal{W} \triangleq \{\mathbf{w}_{n,k}[t]\}$  and the UAV trajectories  $\mathcal{Q} \triangleq \{\mathbf{l}_n^A[t]\}$  over the entire mission duration. The joint optimization problem is mathematically formulated as follows:

$$(\mathbf{P1}) : \max_{\mathcal{Q}, \mathcal{W}} \bar{R} = \frac{1}{T} \sum_{t \in \mathcal{T}} \sum_{n \in \mathcal{N}} \sum_{k \in \mathcal{K}_n[t]} R_k(\mathbf{l}_n^A[t], \mathbf{w}_{n,k}[t]) \quad (13a)$$

$$\text{s.t.} \quad \sum_{k \in \mathcal{K}_n[t]} \|\mathbf{w}_{n,k}[t]\|^2 \leq P_{\max}, \quad \forall n \in \mathcal{N}, \forall t \in \mathcal{T}, \quad (13b)$$

$$\mathbf{l}_n^A[1] = \mathbf{l}_n^S, \quad \mathbf{l}_n^A[T] = \mathbf{l}_n^D, \quad \forall n \in \mathcal{N}, \quad (13c)$$

$$\text{Constraints (2), (3), (4), and (5).} \quad (13d)$$

Constraint (13b) limits the instantaneous transmit power of each UAV, and constraint (13c) enforce the start/end locations of the UAVs.

### D. Problem Decomposition

Problem (P1) poses significant challenges due to its mixed-integer non-convex nature. First, the objective function involves complex coupling between trajectory variables  $\mathbf{l}_n^A[t]$  and beamforming vectors  $\mathbf{w}_{n,k}[t]$  through the non-linear rate expression. Second, and more critically, the user association set  $\mathcal{K}_n[t]$  is a discontinuous function of the UAV locations, making the objective function non-differentiable. To make the problem tractable, we leverage the timescale separation between the rapid fluctuations of small-scale fading channels (milliseconds) and the relatively slow mechanical mobility of UAVs (seconds). Based on this characteristic, we decompose (P1) into two hierarchical subproblems: an inner-loop instantaneous beamforming optimization (P2.1) and an outer-loop long-term trajectory planning (P2.2). The overall proposed solution framework is illustrated in Fig. 2.

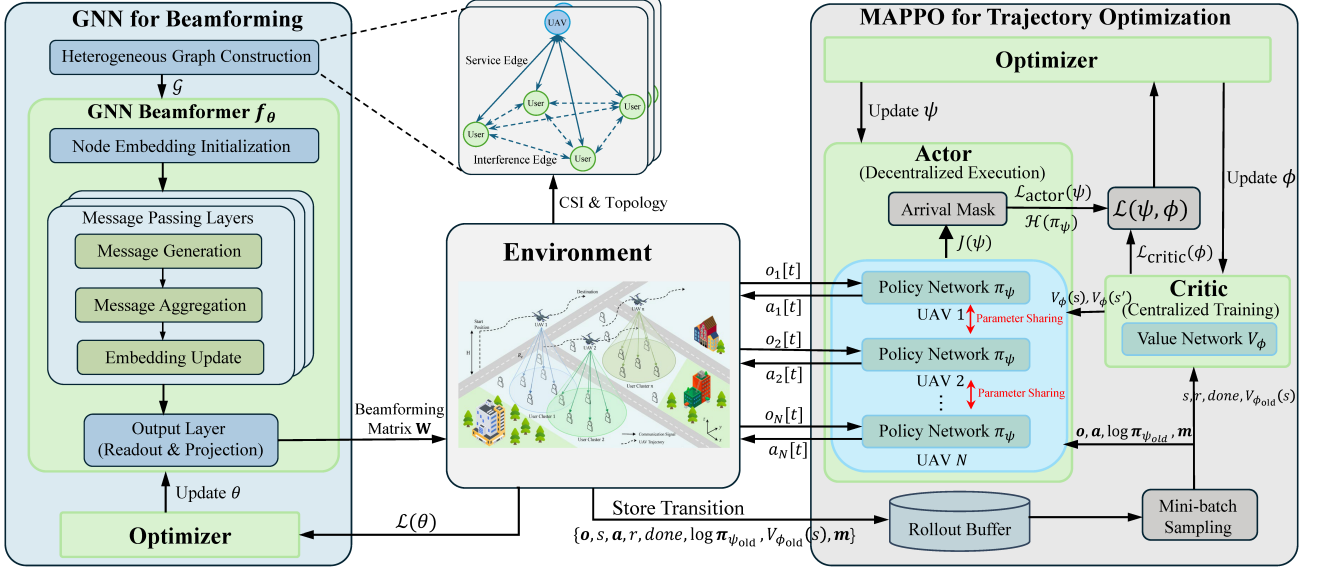


Fig. 2: Overall framework of the proposed GNN-enabled beamforming and MAPPO-based UAV trajectory optimization.

In the inner loop, we focus on a single time slot  $t$ , assuming the UAV locations  $\mathbf{l}_n^A[t]$  are fixed. The objective is to maximize the instantaneous sum rate  $R[t]$  by optimizing the beamforming vectors. This subproblem is formulated as:

$$(\mathbf{P2.1}) : R[t] = \max_{\mathbf{W}} \sum_{n \in \mathcal{N}} \sum_{k \in \mathcal{K}_n[t]} R_k(\mathbf{w}_{n,k}[t]) \quad (14a)$$

$$\text{s.t. } \sum_{k \in \mathcal{K}_n[t]} \|\mathbf{w}_{n,k}[t]\|^2 \leq P_{\max}, \quad \forall n \in \mathcal{N}. \quad (14b)$$

Although **(P2.1)** eliminates trajectory variables, it remains a non-convex problem dominated by complex intra-cluster interference. Conventional iterative solvers typically incur high computational latency, making them unsuitable for real-time channel variations. To address this, we propose a topology-aware GNN beamformer to approximate the optimal solution of **(P2.1)** with low inference latency.

In the outer loop, the goal is to optimize the UAV trajectories  $\mathcal{Q}$  over the entire mission duration to maximize the long-term average sum rate  $\bar{R}$ . This optimization assumes that for any given UAV position, the beamforming vectors are generated by the pre-trained GNN beamformer. The subproblem is formulated as:

$$(\mathbf{P2.2}) : \bar{R} = \max_{\mathcal{Q}} \frac{1}{T} \sum_{t \in \mathcal{T}} \sum_{n \in \mathcal{N}} \sum_{k \in \mathcal{K}_n[t]} R_k(\mathbf{l}_n^A[t]) \quad (15a)$$

$$\text{s.t. } \mathbf{l}_n^A[1] = \mathbf{l}_n^S, \quad \mathbf{l}_n^A[T] = \mathbf{l}_n^D, \quad \forall n \in \mathcal{N}, \quad (15b)$$

$$\text{Constraints (2), (3), (4), and (5).} \quad (15c)$$

Problem **(P2.2)** represents a sequential decision-making process with long-term temporal dependencies and coupled multi-UAV constraints (e.g., collision avoidance). To tackle the exponential complexity, we reformulate **(P2.2)** as a MARL task and employ the MAPPO algorithm.

As shown in Fig. 2, the proposed framework integrates the two modules into a closed loop. The MAPPO agent acts as the high-level planner, determining the UAV movements for

the next time step. The GNN beamformer acts as part of the environment, rapidly calculating the optimal beamforming strategy and the resulting achievable sum rate based on the current topology. This rate serves as part of the immediate reward signal to guide the MAPPO training, enabling the joint optimization of communication and control.

#### IV. GNN-BASED BEAMFORMING

This section details the inner-loop solution for the instantaneous beamforming subproblem **(P2.1)**.

##### A. Heterogeneous Graph Construction

At each time slot  $t$ , the local communication environment of UAV  $n$  is modeled as a time-varying heterogeneous graph  $\mathcal{G}_n[t] = (\mathcal{V}_n[t], \mathcal{E}_n[t])$ . The node set  $\mathcal{V}_n[t]$  comprises two types of nodes: a central UAV node  $v_n$  and  $K_n[t]$  user nodes  $\{u_k\}_{k \in \mathcal{K}_n[t]}$ , where  $K_n[t] = |\mathcal{K}_n[t]|$  denotes the instantaneous number of associated users. The edge set  $\mathcal{E}_n[t]$  constructs a fully connected topology to capture all physical interactions. Implicitly distinguished by node types, edges connecting the UAV  $v_n$  to users  $\{u_k\}$  represent data transmission links, while edges between user pairs  $(u_k, u_j)$  denote interference coupling channels. This unified structure enables the GNN to aggregate global intra-cluster information for effective interference management. Since the optimization is performed per time slot, each time slot corresponds to an independent graph instance. Crucially, all such instances are processed by the same GNN model with shared parameters, enabling the framework to generalize across varying network topologies and user cluster sizes  $K_n[t]$ .

To ensure the model's transferability across different geometric configurations, we design node features based solely on observable CSI. Specifically, for the downlink channel  $\mathbf{h}_{n,k}[t] \in \mathbb{C}^{L \times 1}$ , we decompose the complex-valued vector

into real and imaginary components. The initial feature vector  $\mathbf{x}_k^{(0)}[t] \in \mathbb{R}^{2L}$  for user node  $u_k$  is constructed as [4]:

$$\mathbf{x}_k^{(0)}[t] = [\Re\{\mathbf{h}_{n,k}[t]\}^T, \Im\{\mathbf{h}_{n,k}[t]\}^T]^T. \quad (16)$$

This design strictly adheres to permutation invariance and avoids dependency on specific deployment scenarios (e.g., AoD or user positions), thereby enhancing the robustness and generalization capability of the proposed GNN model.

### B. GNN Architecture with GraphNorm

To effectively handle the time-varying heterogeneous graph scale caused by the mobility of the UAV, we design a GraphNorm-enhanced GNN architecture [34]. Unlike Batch Normalization which relies on batch statistics, GraphNorm normalizes node features based on the statistics of the current graph instance [34], ensuring robust inference across different cluster sizes. We integrate GraphNorm into all multi-layer perceptron (MLP) blocks within the GNN model. For a set of node features  $\mathbf{H} \in \mathbb{R}^{K \times D}$  in a graph instance, where  $K$  denotes the number of nodes and  $D$  represents the feature dimension, GN performs normalization along the node dimension:

$$\text{GN}(\mathbf{h}_{n,k}) = \gamma \odot \frac{\mathbf{h}_{n,k} - \mu}{\sqrt{\sigma^2 + \epsilon}} + \beta, \quad (17)$$

where  $\mu$  and  $\sigma^2$  are the mean and variance computed over the  $K$  nodes in the current graph, and  $\gamma, \beta$  are learnable affine parameters. This operation stabilizes the feature distribution regardless of the instantaneous user number  $K_n[t]$ , which make the GNN model applicable to the time-varying heterogeneous graph.

As shown in Fig. 2, the architecture of the GNN model follows the standard message passing paradigm. The detailed procedures are described as follows:

**1) Node Embedding Initialization:** The raw CSI features  $\mathbf{x}_k^{(0)}$  are projected into high-dimensional user node embeddings  $\mathbf{u}_k^{(0)}$  using a user-shared  $\text{MLP}_{\text{enc}}$ . The UAV node embedding  $\mathbf{a}_n^{(0)}$  is then initialized by aggregating the normalized user embeddings:

$$\mathbf{u}_k^{(0)} = \text{MLP}_{\text{enc}}(\mathbf{x}_k^{(0)}) \in \mathbb{R}^{d_u}, \quad (18)$$

$$\mathbf{a}_n^{(0)} = \text{MLP}_{\text{uav}}\left(\frac{1}{K_n[t]} \sum_{k \in \mathcal{K}_n[t]} \mathbf{u}_k^{(0)}\right) \in \mathbb{R}^{d_a}, \quad (19)$$

where  $d_u = d_a = d_{\text{gnn}}$  denote the embedding dimensions of the user nodes and UAV nodes.

**2) Message Passing Process:** The GNN model consists of  $L_g$  message-passing layers. In the  $\ell$ -th layer, messages of user and UAV nodes are generated using their corresponding message-generation modules:

$$\mathbf{m}_{\mathbf{u}_k}^{(\ell)} = \text{MLP}_{\text{msg}}^{(u)}(\mathbf{u}_k^{(\ell-1)}) \in \mathbb{R}^{d_u}, \quad (20)$$

$$\mathbf{m}_{\mathbf{a}_n}^{(\ell)} = \text{MLP}_{\text{msg}}^{(a)}(\mathbf{a}_n^{(\ell-1)}) \in \mathbb{R}^{d_a}. \quad (21)$$

User nodes aggregate interference information via max pooling to capture the dominant interferer and combine it with the UAV's global guidance:

$$\bar{\mathbf{m}}_{\mathbf{u}_k}^{(\ell)} = \text{concat}\left(\mathbf{m}_{\mathbf{a}_n}^{(\ell)}, \max_{j \in \mathcal{K}_n[t], j \neq k} \mathbf{m}_{\mathbf{u}_j}^{(\ell)}\right) \in \mathbb{R}^{d_u + d_a}. \quad (22)$$

For the UAV node, mean pooling is employed to aggregate the messages from all associated user nodes:

$$\bar{\mathbf{m}}_{\mathbf{a}_n}^{(\ell)} = \frac{1}{K_n[t]} \sum_{k \in \mathcal{K}_n[t]} \mathbf{m}_{\mathbf{u}_k}^{(\ell)} \in \mathbb{R}^{d_u}. \quad (23)$$

Finally, the embeddings of both the user and UAV nodes are updated based on the aggregated messages:

$$\mathbf{u}_k^{(\ell)} = \text{MLP}_{\text{upd}}^{(u)}\left(\mathbf{u}_k^{(\ell-1)}, \bar{\mathbf{m}}_{\mathbf{u}_k}^{(\ell)}\right) \in \mathbb{R}^{d_u}, \quad (24)$$

$$\mathbf{a}_n^{(\ell)} = \text{MLP}_{\text{upd}}^{(a)}\left(\mathbf{a}_n^{(\ell-1)}, \bar{\mathbf{m}}_{\mathbf{a}_n}^{(\ell)}\right) \in \mathbb{R}^{d_a}. \quad (25)$$

This architecture enables representation learning of intra-cluster interference relationships without explicitly constructing edge features.

**3) Beamforming Vector Output:** Finally, the resulting user embedding  $\mathbf{u}_k^{(L_g)}$  is fed into a readout head to generate the beamforming vector  $\tilde{\mathbf{w}}_{n,k}$ :

$$\tilde{\mathbf{w}}_{n,k} = \text{MLP}_{\text{out}}(\mathbf{u}_k^{(L_g)}). \quad (26)$$

The vector  $\tilde{\mathbf{w}}_{n,k}$  is then projected onto the feasible power region to satisfy the transmit power constraint:

$$\alpha_n(t) = \min\left(1, \sqrt{\frac{P_{\max}}{\sum_{k \in \mathcal{K}_n(t)} \|\tilde{\mathbf{w}}_{n,k}(t)\|_2^2 + \varepsilon}}\right), \quad (27)$$

$$\mathbf{w}_{n,k}(t) = \alpha_n(t) \tilde{\mathbf{w}}_{n,k}(t), \quad (28)$$

where  $\varepsilon$  is a numerical stability term introduced to avoid numerical instability or gradient explosion when the total unnormalized beamforming power approaches zero. This projection operation guarantees that the output beamforming vectors always satisfy the transmit power constraint while preserving end-to-end differentiability.

### C. Training and Complexity Analysis

Instead of relying on labeled data generated by computationally expensive iterative solvers, we adopt a reward-driven learning paradigm that aligns with the principles of RL. In this context, the GNN beamformer  $f_{\theta}$  functions as a policy network, which directly maps the environmental state (i.e., the channel CSI) to the optimal action (i.e., beamforming vectors). The network parameters  $\theta$  are optimized via stochastic gradient descent (SGD) to maximize the instantaneous reward, defined as the system sum rate. Formally, let  $\mathcal{D}_{\text{gnn}}$  denote the training dataset consisting of clustered channel samples. During the training phase, we sample a mini-batch  $\mathcal{B}_{\text{gnn}}$  of size  $B_{\text{gnn}}$ . Since each user cluster constitutes an independent graph instance, the training objective is to maximize the average expected reward  $\bar{R}_{\text{clus}}(\theta)$  over the mini-batch, which is defined as:

$$\bar{R}_{\text{clus}}(\theta) = \frac{1}{B_{\text{gnn}} \times N} \sum_{m \in \mathcal{B}_{\text{gnn}}} \sum_{n \in \mathcal{N}} \sum_{k \in \mathcal{K}_{m,n}} R_k(\mathbf{W}_{m,n}), \quad (29)$$

where  $\mathbf{W}_{m,n}$  is the beamforming matrix generated by  $\mathbf{W}_{m,n} = f_{\theta}(\mathbf{H}_{m,n})$  and  $\mathbf{H}_{m,n}$  represents the CSI matrix of the  $n$ -th cluster in sample  $m$ . The loss function is defined as:

$$\mathcal{L}(\theta) = -\bar{R}_{\text{clus}}(\theta), \quad (30)$$

---

**Algorithm 1** GNN Training

---

**Input:** Clustered dataset  $\mathcal{D}_{\text{gnn}}$ , UAV number  $N$ , batch size  $B_{\text{gnn}}$ , epoch number  $E_{\text{gnn}}$ , GNN beamformer  $f_{\theta}$ ;  
**Output:** Trained parameters  $\theta$ ;

- 1: Initialize GNN beamformer  $f_{\theta}$ ;
- 2: Load clustered dataset  $\mathcal{D}_{\text{gnn}} = \{\mathcal{C}_m\}_{m=1}^M$  where each sample  $m$  has clusters  $\mathcal{C}_m = \{\mathbf{H}_{m,n}\}_{n=1}^N$ ;
- 3: **for** epoch = 1 to  $E_{\text{gnn}}$  **do**
- 4:   Shuffle sample indices;
- 5:   **for** each mini-batch  $\mathcal{B}_{\text{gnn}}$  **do**
- 6:     Extract all clusters in  $\mathcal{B}_{\text{gnn}}$  into list  $\mathcal{C}$ ;
- 7:      $L_{\text{sum}} \leftarrow 0$ ,  $C_{\text{cnt}} \leftarrow 0$ ;
- 8:     **for** each cluster in  $\mathcal{C}$  **do**
- 9:       Output the beamforming matrix with  $f_{\theta}$ :
- 10:        $\mathbf{W}_{m,n} \leftarrow f_{\theta}(\mathbf{H}_{m,n})$ ;
- 11:       Compute cluster sum-rate loss  $\mathcal{L}_{m,n}$ ;
- 12:       Update  $\mathcal{L}_{\text{sum}}$ ,  $C_{\text{cnt}}$ :
- 13:        $\mathcal{L}_{\text{sum}} \leftarrow \mathcal{L}_{\text{sum}} + \mathcal{L}_{m,n}$ ,  $C_{\text{cnt}} \leftarrow C_{\text{cnt}} + 1$ ;
- 14:     **end for**
- 15:      $\mathcal{L}(\theta) \leftarrow \mathcal{L}_{\text{sum}}/C_{\text{cnt}}$ ;
- 16:     Update  $\theta$  with  $\mathcal{L}_{\text{batch}}$ :
- 17:      $\theta \leftarrow \theta - \eta \nabla_{\theta} \mathcal{L}(\theta)$ ;
- 18:   **end for**
- 19: **end for**

---

The detailed training procedure is outlined in Algorithm 1. To enhance training efficiency, a cluster-level batching strategy is employed. Specifically, since the interference is localized within each cluster, multiple clusters from different time slots are flattened into a single batch. This allows the GNN to process diverse topology instances in parallel, significantly improving sample efficiency and convergence speed.

The computational complexity is dominated by the message passing process. Node updates incur a cost of  $\mathcal{O}(L_g(N + K)d_{\text{gnn}}^2)$ , while message aggregation scales with the total number of edges  $|\mathcal{E}|$  as  $\mathcal{O}(L_g|\mathcal{E}|d_{\text{gnn}})$ . Since the edges are strictly restricted to intra-cluster connections with a limited cluster size  $K_n$ ,  $|\mathcal{E}|$  scales linearly with the total user number  $K$  (i.e.,  $|\mathcal{E}| \propto K$ ). This yields an overall complexity of  $\mathcal{O}(K)$ , ensuring scalability.

## V. MAPPO-BASED MULTI-UAV TRAJECTORY PLANNING

This section elaborates on the outer-loop solution for the long-term trajectory planning subproblem (**P2.2**).

### A. Utilization of Beamforming Results

As shown in Fig. 2, the pre-trained GNN beamformer is integrated into the environment to provide real-time performance feedback. Specifically, at each time step  $t$ , for any given UAV locations, the GNN maps the current CSI matrix  $\mathbf{H}[t]$  to the beamforming vectors  $\mathbf{W}[t]$  by  $\mathbf{W}[t] = f_{\theta}(\mathbf{H}[t])$ . Subsequently, the system calculates the instantaneous sum rate  $R[t]$  based on  $\mathbf{W}[t]$ , which serves as part of the reward signal for the MARL agents (detailed in Section V-B).

This mechanism encapsulates the underlying interference management, allowing the MAPPO agents to optimize long-term trajectories based solely on the observed states and the GNN-feedback rewards.

### B. Dec-POMDP Modeling

We formulate the cooperative multi-UAV trajectory planning problem as a Dec-POMDP, defined by the tuple  $\mathcal{M} = \langle \mathcal{N}, \mathcal{S}, \{\mathcal{A}_n\}, \{\mathcal{O}_n\}, \mathcal{P}, \mathcal{R}, \gamma \rangle$ . Here,  $\mathcal{N}$  is the set of UAV agents. At time slot  $t$ ,  $s[t] \in \mathcal{S}$  denotes the global state. Each agent  $n$  selects an action  $a_n[t] \in \mathcal{A}_n$  based on its local observation  $o_n[t] \in \mathcal{O}_n$ .  $\mathcal{P}$  is the state transition probability,  $\mathcal{R}$  is the reward function, and  $\gamma$  is the discount factor. The detailed components are defined as follows:

1) *Global State*: The global state  $s[t]$  encapsulates the geometric configuration of the entire network, including the locations of all UAVs, users, and destinations. It is defined as:

$$s[t] = \left\{ \{\mathbf{l}_n^A[t]\}_{n \in \mathcal{N}}, \{\mathbf{l}_k^U\}_{k \in \mathcal{K}}, \{\mathbf{l}_n^D\}_{n \in \mathcal{N}} \right\}. \quad (31)$$

This global information is exclusively available to the Critic network during the centralized training phase to facilitate value function estimation.

2) *Local Observation*: To enable decentralized execution, the local observation  $o_n[t]$  of UAV  $n$  relies solely on local information. It consists of its own position, the relative locations of users and the destination, and historical action information:

$$o_n[t] = \{\mathbf{l}_n^A[t], \Delta \mathbf{l}_{n,\text{avg}}^U[t], \Delta \mathbf{l}_n^D[t], \mathbf{a}_n[t-1]\}. \quad (32)$$

Here,  $\Delta \mathbf{l}_{n,\text{avg}}^U[t]$  represents the average relative displacement to all ground users, calculated as  $\frac{1}{K} \sum_{k \in \mathcal{K}} (\mathbf{l}_k^U - \mathbf{l}_n^A[t])$ . This compact representation provides a directional cue toward user-dense regions without expanding the observation dimension as  $K$  increases.  $\Delta \mathbf{l}_n^D[t] \triangleq \mathbf{l}_n^D - \mathbf{l}_n^A[t]$  is the vector pointing to the destination. Additionally, the one-hot encoded previous action  $\mathbf{a}_n[t-1]$  is included to promote trajectory smoothness.

3) *Action Space*: We adopt a discrete action space for UAV  $n$ , which is defined as:

$$\mathcal{A}_n = \{\text{UP}, \text{DOWN}, \text{LEFT}, \text{RIGHT}, \text{STAY}\}. \quad (33)$$

These actions correspond to planar displacement vectors  $\mathbf{D} \in \{(\pm D_{\text{fly}}, 0, 0), (0, \pm D_{\text{fly}}, 0), (0, 0, 0)\}$ , where  $D_{\text{fly}} \triangleq V \delta_t$  denotes the step size determined by the fly speed. The position update rule is given by  $\mathbf{l}_n^A[t+1] = \mathbf{l}_n^A[t] + \mathbf{d}(\mathbf{a}_n[t])$ .

4) *Reward Function*: The reward function is meticulously designed to guide the agents toward a balance between maximizing system sum rate and ensuring safe, timely mission completion. The global reward  $r[t]$  at time slot  $t$  is formulated as a weighted sum of heterogeneous objectives:

$$r[t] = w_{\text{rate}} \bar{R}[t] + w_{\text{arr}} N_{\text{arr}}[t] - w_{\text{bud}} N_{\text{bud}}[t] - w_{\text{col}} N_{\text{col}}[t] + w_{\text{fea}} \sum_{n \in \mathcal{N}} \Phi_n[t]. \quad (34)$$

Here, the integer terms  $N_{\text{arr}}[t]$ ,  $N_{\text{bud}}[t]$ , and  $N_{\text{col}}[t]$  represent the number of UAVs that have newly arrived at destinations, violated boundary constraints, or incurred collisions at the current slot, respectively. The coefficients  $w_{(\cdot)}$  are hyperparameters governing the relative importance of these factors.

To prioritize long-term network performance, the communication component  $\bar{R}[t]$  tracks the cumulative average sum rate achieved up to time  $t$ :

$$\bar{R}[t] = \frac{1}{t} \sum_{\tau=1}^t R[\tau]. \quad (35)$$

Standard trajectory planning suffers from sparse rewards, as agents receive positive feedback only upon reaching the destination, making intermediate decisions difficult to optimize. To address this, the proposed reachability term  $\Phi_n[t]$  provides dense, step-wise supervision by immediately checking physical feasibility at every time slot, effectively guiding the agent to correct its trajectory continuously throughout the flight. Let  $T_n^{\min}[t] = \lceil \|l_n^D - l_n^A[t]\|/D_{\text{fly}} \rceil$  denote the minimum time slots required to reach the destination from the current position, and let  $T_n^{\text{res}}[t] = T_{\max} - t$  be the remaining time. The feasibility indicator is defined as:

$$\Phi_n[t] = \begin{cases} +1, & \text{if } T_n^{\min}[t] \leq T_n^{\text{res}}[t] \wedge T_n^{\min}[t] \leq T_n^{\min}[t-1], \\ -1, & \text{otherwise.} \end{cases} \quad (36)$$

This mechanism rewards agents for maintaining a feasible trajectory while approaching the target, and imposes penalties when deviations make the mission theoretically impossible to complete within the remaining time.

### C. MAPPO with CTDE Framework

1) **Network Architecture:** As shown in Fig. 2, we implement a parameter-sharing Actor-Critic architecture, where all UAV agents share the same set of parameters for both the policy network (Actor) and the value network (Critic). This design not only significantly reduces the model complexity but also promotes the learning of cooperative behaviors by aggregating experiences from all agents.

**Decentralized Actor (Execution Phase):** The Actor network, parameterized by  $\psi$ , serves as the local execution policy for each UAV. It maps the local observation to a stochastic action distribution, which is denoted as  $\pi_\psi(a_n[t] | o_n[t])$ . Crucially, the policy depends solely on the local observation  $o_n[t]$ . This ensures that during the flight phase, each UAV operates autonomously without requiring real-time global information exchange, thereby enabling practical distributed deployment with minimal communication overhead.

**Centralized Critic (Training Phase):** The Critic network, parameterized by  $\phi$ , is employed exclusively during the offline training phase to estimate the state value function, which is denoted as  $V_\phi(s[t])$ . Unlike the Actor, the Critic is conditioned on the global state  $s[t]$ , which provides a stable and accurate return estimation for credit assignment, effectively mitigating the non-stationarity issue and stabilizing the gradient updates.

2) **Optimization Objectives:** The network parameters are updated using the MAPPO algorithm.

**Generalized Advantage Estimation (GAE):** To reduce the variance of gradient estimation while maintaining an acceptable bias, we employ GAE to compute the advantage function. The temporal-difference (TD) error  $\delta_t$  at time step  $t$  is defined as:

$$\delta_t = r[t] + \gamma(1 - \text{done}[t+1])V_\phi(s[t+1]) - V_\phi(s[t]), \quad (37)$$

where  $\text{done}[t+1] \in \{0, 1\}$  serves as a termination mask that zeros out the discounted future value if the episode concludes at step  $t+1$ . The advantage estimate  $\hat{A}_t$  is given by the exponentially weighted sum of TD errors:

$$\hat{A}_t = \sum_{l=0}^{\infty} (\gamma \lambda)^l \delta_{t+l}, \quad (38)$$

where  $\lambda \in [0, 1]$  is the GAE smoothing factor governing the bias-variance trade-off.

**Masked Actor Loss:** The Actor network  $\pi_\psi$  is updated by maximizing the clipped surrogate objective. However, in the multi-UAV scenario, agents may reach their destinations at different time steps. Once a UAV completes its task, its subsequent actions (typically STAY) are deterministic and should not influence the policy gradient. To address this, we introduce a binary active agent mask  $m_{n,t} \in \{0, 1\}$ , where  $m_{n,t} = 0$  indicates that UAV  $n$  has finished its mission. First, let  $J_{n,t}(\psi)$  denote the standard clipped surrogate objective for a specific agent  $n$  at time step  $t$ :

$$J_{n,t}(\psi) = \min \left( \rho_{n,t} \hat{A}_{n,t}, \text{clip}(\rho_{n,t}, 1 - \epsilon, 1 + \epsilon) \hat{A}_{n,t} \right), \quad (39)$$

where  $\rho_{n,t}(\psi) = \frac{\pi_\psi(a_n[t]|o_n[t])}{\pi_{\psi_{\text{old}}}(a_n[t]|o_n[t])}$  is the probability ratio and  $\epsilon$  is the clipping parameter. Based on this, the final masked actor loss is defined as the negative average of these objectives over active agents in the mini-batch  $\mathcal{B}_{\text{ppo}}$ :

$$\mathcal{L}_{\text{actor}}(\psi) = -\frac{1}{\sum_{n \in \mathcal{N}} \sum_{t \in \mathcal{B}_{\text{ppo}}} m_{n,t}} \sum_{n \in \mathcal{N}} \sum_{t \in \mathcal{B}_{\text{ppo}}} m_{n,t} \cdot J_{n,t}(\psi). \quad (40)$$

This masking mechanism ensures that the policy optimization focuses exclusively on meaningful decision-making processes, effectively filtering out noise from completed agents.

**Critic Loss and Total Objective:** The critic network  $V_\phi$  is updated to minimize the mean squared error between the value prediction and the estimated return. To prevent destructive updates caused by excessive changes in value estimation, the clipped value loss technique is adopted. Let  $\hat{R}_t = \hat{A}_t + V_{\phi_{\text{old}}}(s[t])$  denote the target return. The clipped value prediction  $\tilde{V}_{\phi,t}$  is explicitly formulated to restrict the new value estimate within a trusted region:

$$\tilde{V}_{\phi,t} = V_{\phi_{\text{old}}}(s[t]) + \text{clip}(V_\phi(s[t]) - V_{\phi_{\text{old}}}(s[t]), -\epsilon, \epsilon). \quad (41)$$

The critic loss is then calculated as the maximum of the unclipped and clipped squared errors:

$$\mathcal{L}_{\text{critic}}(\phi) = \frac{1}{|\mathcal{B}_{\text{ppo}}|} \sum_{t \in \mathcal{B}_{\text{ppo}}} \max \left[ \left( V_\phi(s[t]) - \hat{R}_t \right)^2, \left( \tilde{V}_{\phi,t} - \hat{R}_t \right)^2 \right]. \quad (42)$$

Finally, the total optimization objective is constructed as a weighted combination of the actor loss, critic loss, and entropy regularization:

$$\mathcal{L}_{\text{total}}(\psi, \phi) = \mathcal{L}_{\text{actor}}(\psi) + c_1 \mathcal{L}_{\text{critic}}(\phi) - c_2 \mathcal{H}(\pi_\psi), \quad (43)$$

where  $c_1$  and  $c_2$  represent the value loss coefficient and entropy coefficient, respectively. The entropy term  $\mathcal{H}(\pi_\psi)$  is

**Algorithm 2** MAPPO Training

**Input:** Pre-trained GNN beamformer  $f_\theta$ , Actor–Critic networks  $(\pi_\psi, V_\phi)$ , total training steps  $T_{\text{total}}$ , rollout length  $T_{\text{rollout}}$ , discount factor  $\gamma$ , GAE smoothing factor  $\lambda$ , PPO clipping factor  $\epsilon$ , update epoch number  $E_{\text{ppo}}$ , mini-batch size  $B_{\text{ppo}}$ ;

**Output:** Policy parameters  $\psi$  and value parameters  $\phi$ ;

- 1: Initialize shared-parameter Actor–Critic  $(\pi_\psi, V_\phi)$ ;
- 2: Reset environment, obtain initial observations  $\mathbf{o}[0] = \{o_n[0]\}_{n \in \mathcal{N}}$  and global state  $s[0]$ ;
- 3: **for** step number = 1 to  $T_{\text{total}}$  **do**
- 4:   Initialize rollout buffer  $\mathcal{D}_{\text{ppo}}$ ;
- 5:   **for**  $t = 0$  to  $T_{\text{rollout}} - 1$  **do**
- 6:     **for** each UAV  $n \in \mathcal{N}$  **do**
- 7:       **if** UAV  $n$  has arrived **then**
- 8:          $a_n[t] \leftarrow \text{STAY}$ ,  $m_{n,t} \leftarrow 0$ ;
- 9:       **else**
- 10:         Sample  $a_n[t] \sim \pi_\psi(\cdot | o_n[t])$ , set  $m_{n,t} \leftarrow 1$ ;
- 11:       **end if**
- 12:     **end for**
- 13:     Execute joint action  $\mathbf{a}[t]$ , observe rewards  $\mathbf{r}[t]$ , termination  $done[t]$ , next observations  $\mathbf{o}[t+1]$ , and state  $s[t+1]$ ;
- 14:     Store transition  $\{o_n[t], s[t], a_n[t], r[t], done[t], \log \pi_{\psi_{\text{old}}}(a_n[t] | o_n[t]), V_{\phi_{\text{old}}}(s[t]), m_{n,t}\}$  into  $\mathcal{D}_{\text{ppo}}$ ;
- 15:   **end for**
- 16:   Compute GAE advantages  $\hat{A}_t$  and returns  $\hat{R}_t$ ;
- 17:   **for** epoch = 1 to  $E_{\text{ppo}}$  **do**
- 18:     Shuffle data in  $\mathcal{D}_{\text{ppo}}$  and split into mini-batches;
- 19:     **for** each mini-batch  $\mathcal{B}_{\text{ppo}} \in \mathcal{D}_{\text{ppo}}$  **do**
- 20:       Compute  $\mathcal{L}_{\text{actor}}(\psi)$ ,  $\mathcal{L}_{\text{critic}}(\phi)$ , and  $\mathcal{L}_{\text{total}}(\psi, \phi)$ ;
- 21:       Update  $(\psi, \phi)$  by minimizing  $\mathcal{L}_{\text{total}}(\psi, \phi)$ :
- 22:        $(\psi, \phi) \leftarrow (\psi, \phi) - \alpha \nabla_{\psi, \phi} \mathcal{L}_{\text{total}}(\psi, \phi)$ ;
- 23:     **end for**
- 24:   **end for**
- 25: **end for**

incorporated to encourage exploration by preventing the policy from becoming deterministic too early, thereby mitigating the risk of premature convergence to suboptimal local optima.

#### D. Training and Complexity Analysis

The complete training workflow, summarized in Algorithm 2, alternates between rollout collection and parameter optimization. During the rollout phase, agents interact with the environment under an arrival-aware sampling scheme, which locks completed agents to the STAY action to prevent invalid exploration. Upon collecting trajectories, the centralized Critic estimates advantages via GAE, and the shared parameters  $(\psi, \phi)$  are subsequently updated using mini-batch SGD for  $E_{\text{ppo}}$  epochs.

For the trajectory planning subproblem, the complexity is dominated by the observation processing and the forward propagation of the Actor network. Specifically, constructing the local observation  $o_n[t]$  involves calculating the relative average user location  $\Delta l_{n, \text{avg}}^U[t]$ , which requires aggregating coordinates from all  $K$  users, leading to a complexity of  $\mathcal{O}(K)$ . Subse-

**TABLE I: Simulation Parameters**

Parameter	Value
GNN Embedding Dimension ( $d_{\text{gnn}}$ )	128
Number of GNN Message-Passing Layers ( $L_g$ )	3
GNN Learning Rate ( $\eta$ )	$1 \times 10^{-3}$
GNN Weight Decay	$1 \times 10^{-6}$
MAPPO Learning Rate ( $\alpha$ )	$3 \times 10^{-4}$
MAPPO Discount Factor ( $\gamma$ )	0.99
MAPPO GAE Smoothing Factor ( $\lambda$ )	0.95
MAPPO Clip Coefficient ( $\epsilon$ )	0.2
MAPPO Value Loss & Entropy Coefficient ( $c_1$ & $c_2$ )	0.5 & 0.01

quently, the Actor network maps the observation to an action with a constant complexity of  $\mathcal{O}(L_a d_{\text{actor}}^2)$ . Although the total computational complexity for  $N$  UAVs is  $\mathcal{O}(N(K + L_a d_{\text{actor}}^2))$ , the proposed CTDE framework enables parallel decentralized execution. Thus, the critical inference latency is determined by the single-agent complexity  $\mathcal{O}(K + L_a d_{\text{actor}}^2) \approx \mathcal{O}(K)$ . Combining this with the GNN-based beamforming complexity of  $\mathcal{O}(K)$  derived in Section IV-C, the overall per-slot decision latency scales linearly with  $K$ . This linear scalability constitutes a significant advantage over the polynomial complexity of conventional iterative algorithms, ensuring feasibility for real-time deployment in highly dynamic networks.

## VI. SIMULATION RESULTS

### A. Simulation Settings

We consider a multi-UAV downlink communication network deployed within a square mission area of  $200 \times 200$  m<sup>2</sup>. The ground users are randomly distributed within the area, while the UAVs are initialized at starting locations. Each UAV is equipped with a ULA consisting of  $L = 4$  antennas with half-wavelength spacing ( $d_a = \lambda/2$ ). The maximum transmit power of each UAV is  $P_{\text{max}} = 30$  dBm, and the maximum communication coverage radius is set to  $R_c = 150$  m. The wireless channel follows the LoS channel model described in Section III, with a reference channel gain of  $\beta_0 = -20$  dB at  $d_0 = 1$  m and a noise power of  $\sigma_0^2 = -90$  dBm.

The proposed hierarchical framework is trained in two stages. First, for the GNN-based beamforming, the architecture comprises  $L_g = 3$  message-passing layers. We generate a training dataset consisting of 10,000 clustered channel snapshots. The model is trained using the Adam optimizer for  $E_{\text{gnn}} = 25$  epochs to ensure convergence. Then, for the MAPPO-based trajectory planning, the agents interact with the environment for a total of  $T_{\text{total}} = 2 \times 10^6$  time steps. The training utilizes a rollout buffer of length  $T_{\text{rollout}} = 256$  steps. In each update iteration, the collected trajectories are divided into 4 mini-batches, and the actor-critic networks are updated for  $E_{\text{ppo}} = 10$  epochs. The detailed simulation parameters and hyperparameter settings are summarized in Table I.

### B. Beamforming Performance Comparison

To comprehensively evaluate the efficacy and robustness of the proposed GNN-based beamformer, we benchmark

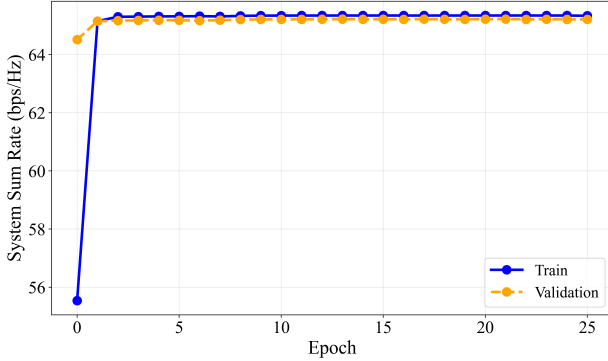


Fig. 3: Average sum rate on training and validation datasets across epochs.

it against three representative algorithms, including a high-performance heuristic solver and two state-of-the-art deep learning architectures:

- 1) **Genetic Algorithm (GA) [35]:** A heuristic algorithm that extensively searches the solution space to handle non-convexity. We employ the GA provided by PYMOO [36], configured with 2,000 generations, to provide an approximate performance upper bound for quantifying the optimality gap.
- 2) **DeepSets [37]:** A fundamental architecture based on deep neural network designed for set-structured data. It ensures permutation invariance by encoding individual user features and aggregating them via a global max-pooling operation.
- 3) **Multi-Scale PointNet (MS-PointNet) [38]:** Based on convolutional neural network, this model adapt from point cloud processing and employ parallel 1-D convolutions with varying kernel sizes (e.g. 1,3,5) to capture multi-scale features while maintaining permutation invariance.

To evaluate the scalability and generalization capability, all learning-based models (Proposed GNN, DeepSets, and MS-PointNet) are trained on a network consisting of  $K = 3$  UAVs and  $U = 12$  users. Once trained, the model parameters are fixed and directly deployed to various test scenarios (e.g., varying UAV/user numbers) without re-training. This setup strictly tests whether the models have learned the underlying interference management rules rather than merely overfitting to a specific network size.

1) *Convergence Analysis:* Fig. 3 illustrates the convergence performance on both training and validation datasets. The model exhibits rapid convergence to a near-optimal sum rate ( $\approx 65$  bps/Hz) within the first few epochs. Crucially, the negligible gap between the training and validation curves confirms that the proposed GNN effectively captures generic interference patterns with robust generalization capabilities, avoiding overfitting.

2) *Performance Comparison under Varying Channel Conditions:* To further evaluate the robustness of the proposed GNN beamformer, we examine the sum rate with respect to the maximum transmit power  $P_{\max}$  and the noise power  $\sigma_0^2$ .

Fig. 4 plots the sum rate against  $P_{\max}$ . A distinct performance divergence emerges in the high-power regime: the proposed GNN consistently tracks the GA upper bound ( $\approx 80$

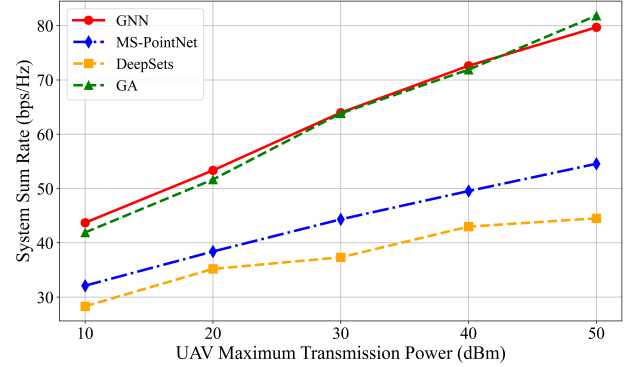


Fig. 4: Sum rate versus UAV maximum transmission power.

bps/Hz at 50 dBm), whereas MS-PointNet and DeepSets saturate early at 55 and 45 bps/Hz, respectively. This saturation occurs because the network shifts into an interference-dominated phase. The baselines rely on global max-pooling, which compresses user-specific features into a fixed-size vector, thereby losing the structural granularity required for precise interference nulling. In contrast, the GNN leverages message passing to explicitly capture pairwise interference couplings, enabling effective suppression even under strong interference.

Fig. 5 depicts system robustness against noise power. The GNN demonstrates exceptional resilience, maintaining statistical parity with the GA bound even in high-noise settings ( $-70$  dBm). Conversely, the baselines lag behind by a substantial margin of 15–20 bps/Hz. This gap highlights the limitations of structure-agnostic architectures: without explicit topology modeling, they struggle to distinguish interference patterns from background noise. By preserving structural information via message passing, the GNN ensures robust beamforming regardless of SINR degradation.

3) *Generalization Capability:* To validate the generalization capability, we perform generalization tests by applying the pre-trained GNN, DeepSets, and MS-PointNet models directly to scenarios with varying number of UAVs and users.

Fig. 6 plots the system sum rate as the UAV number  $N$  increases from 2 to 6. The proposed GNN demonstrates robust scalability by tightly tracking the GA upper bound. This success is attributed to the permutation-equivariant nature of the graph architecture: adding a UAV simply corresponds to instantiating a new node, allowing the learned message-passing rules to effectively coordinate interference regardless of network size. In contrast, DeepSets and MS-PointNet exhibit a widening optimality gap, as their global aggregation mechanisms fail to capture the pairwise interference dependencies that grow quadratically with  $N$ .

Fig. 7 illustrates the impact of increasing user number  $K$  from 8 to 28, revealing a fundamental divergence in algorithmic behaviors. Remarkably, in the high-density regime ( $K > 16$ ), the GNN outperforms the GA. This counter-intuitive result highlights the curse of dimensionality in heuristic optimization: while the search space expands exponentially with  $K$ , rendering GA's fixed generation budget (2000 generations) insufficient, the GNN relies on learned local interference management rules rather than global search, enabling superior inference in

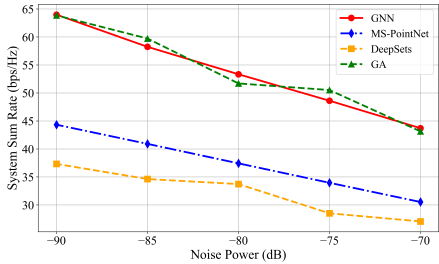


Fig. 5: Sum rate vs. noise power.

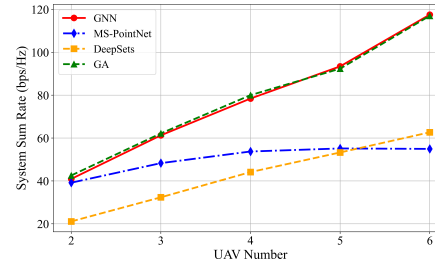


Fig. 6: Sum rate vs. user number.

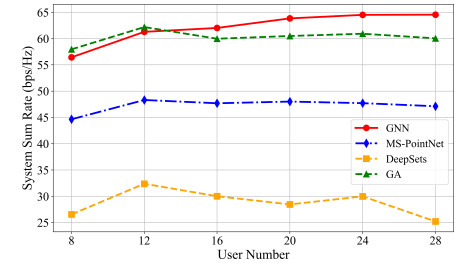


Fig. 7: Sum rate vs. the user number.

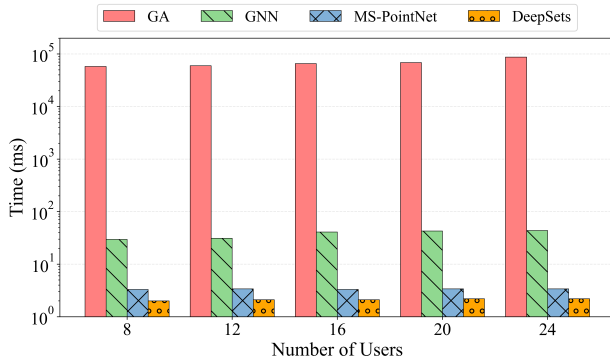


Fig. 8: Average computation time per beamforming decision.

dense networks. Conversely, DeepSets exhibits an anomalous downward trend, while MS-PointNet struggles to achieve significant gains. Theoretically, increasing users should yield multi-user diversity gains. However, the core limitation of DeepSets lies in its information bottleneck: its global pooling operation forces the compression of all  $K$  user channels into a fixed-size latent vector. In dense networks, this compression is too aggressive—it blurs out the fine-grained spatial details. As a result, the model loses the precise angular information needed to separate closely spaced users and block interference. Similarly, although MS-PointNet extracts local features, it lacks explicit edge-level message passing to map interferers to victims. Consequently, the severe intra-cluster interference caused by imprecise beamforming leads to the observed performance degradation.

4) *Computational Complexity Analysis*: To assess real-time feasibility, Fig. 8 compares the average inference latency per decision on a logarithmic scale. The GA requires  $5.8 \times 10^4$  to  $8.7 \times 10^4$  ms (58–87 s) due to iterative population evolution. This prohibitive latency far exceeds the coherence time of high-mobility A2G channels, rendering GA impractical for online deployment where CSI expires within milliseconds. In contrast, the proposed GNN achieves a stable inference time of 30–45 ms, representing a speedup of three orders of magnitude ( $\approx 2000\times$ ) over GA. Crucially, the computational overhead exhibits excellent scalability with respect to network density. As the number of users increases from 8 to 24, the GNN inference time grows only marginally from 29.6 ms to 43.8 ms. This linear and modest increase confirms that the graph-based inference remains computationally efficient even in dense networks. While DeepSets and MS-PointNet achieve lower latencies (2–4 ms) via simplistic global pooling, they suffer

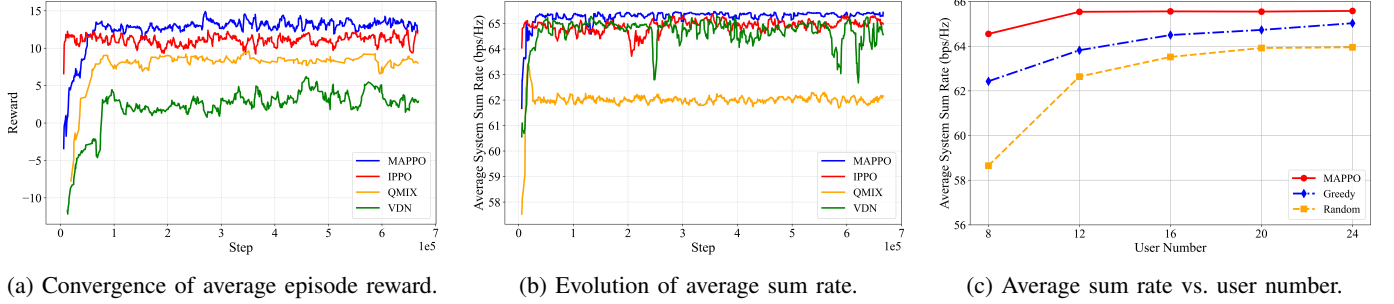
from severe performance degradation in dense networks (as shown in Fig. 7). Since the GNN’s latency remains well within the typical channel coherence window, it strikes the optimal balance between computational efficiency and beamforming accuracy.

### C. Trajectory Planning Performance Comparison

Having established thorough performance evaluation of the GNN beamformer, we now proceed to evaluate the proposed MAPPO-based trajectory planning algorithm. To strictly isolate the contributions of path planning strategies, it is worth emphasizing that the same pre-trained GNN beamformer (validated in Section VI-B) is deployed as the fixed underlying beamformer to generate reward feedback for all compared baselines. By fixing the beamforming module, this setup ensures that any performance divergence is solely attributable to the efficacy of the trajectory policies rather than variations in channel estimation.

We simulate a mission scenario involving 3 UAVs navigating from fixed starting locations  $\mathbf{l}_s$  to their respective destinations  $\mathbf{l}_d$ . Specifically, the coordinates are set as  $\mathbf{l}_s = \{[20, 20, 100]^T, [20, 180, 100]^T, [180, 180, 100]^T\}$  and  $\mathbf{l}_d = \{[180, 100, 100]^T, [180, 20, 100]^T, [20, 100, 100]^T\}$ . The discrete flight step size is fixed at  $D_{\text{fly}} = 20$  m, and a minimum safety distance of  $D_{\text{min}} = 25$  m is strictly enforced to prevent collisions. The maximum mission horizon is set to  $T_{\text{max}} = 24$  time steps. To evaluate the superiority of the proposed MAPPO framework, we compare it against five distinct baselines including independent learning, value decomposition, and heuristic strategies:

- 1) **Independent PPO (IPPO) [7]:** A fully decentralized baseline where agents optimize policies based solely on local observations. It serves as a reference to validate the necessity of centralized training.
- 2) **VDN [39]:** A value-based CTDE method that assumes the joint action-value function  $Q_{\text{tot}}$  can be additively decomposed into local value functions, i.e.,  $Q_{\text{tot}} = \sum_{n=1}^K Q_n$ .
- 3) **QMIX [40]:** An advancement over VDN that employs a hypernetwork to mix local  $Q$ -values in a non-linear manner. It enforces a monotonicity constraint ( $\frac{\partial Q_{\text{tot}}}{\partial Q_n} \geq 0$ ) to ensure consistency between local greedy actions and the global optimum within the CTDE paradigm.
- 4) **Greedy Strategy:** A heuristic approach where UAVs exhaustively search the joint action space at each time step to maximize the instantaneous system sum rate.



(a) Convergence of average episode reward.

(b) Evolution of average sum rate.

(c) Average sum rate vs. user number.

Fig. 9: Performance evaluation of the proposed MAPPO-based trajectory planning algorithm: (a) Training convergence comparison, (b) Long-term sum rate evolution, and (c) Scalability against varying user densities.

### 5) Random Strategy: A lower-bound baseline where UAVs select actions stochastically.

To ensure a rigorous and fair comparison, all MARL-based algorithms (i.e., MAPPO, IPPO, VDN, and QMIX) share the modeling and weight settings as detailed in Section V-A, differing only in their learning paradigms. For the heuristic baselines (Greedy and Random), a mandatory reachability constraint is enforced: any action that would render the destination unreachable within the remaining time budget is masked out. This guarantees that all UAVs can arrive at their destinations within  $T_{\max}$ .

1) *Convergence Analysis*: Fig. 9a depicts the convergence curves of the average episode reward for the proposed MAPPO algorithm against three MARL benchmarks: IPPO, QMIX, and VDN.

A detailed inspection of the learning dynamics reveals a distinct trade-off between initial speed and long-term optimality. IPPO exhibits a rapid initial surge, outperforming MAPPO within the first  $5 \times 10^4$  steps. This phenomenon is attributed to the myopic greedy nature of independent learners, which can quickly learn the local optimal actions. However, by ignoring the non-stationarity induced by other agents, IPPO fails to master cooperative evasion maneuvers, leading to premature convergence to local optima (rewards plateauing around 11–12). In contrast, MAPPO demonstrates superior long-term potential. Although the centralized critic requires more samples to accurately estimate the global value function initially, it eventually guides the UAVs to learn sophisticated cooperative strategies, such as collision avoidance. Consequently, MAPPO breaks through the performance bottlenecks of independent learning, stabilizing at the highest reward interval (13–14).

Furthermore, the results highlight the advantage of policy-based methods over value-decomposition approaches in this domain. VDN yields the most unstable performance, suggesting that its linear value decomposition assumption is fundamentally insufficient to approximate the highly non-linear interference topology. While QMIX improves upon this via non-linear mixing, it still lags significantly behind the policy gradient-based algorithms. This indicates that for long-term trajectory planning tasks with complex coupled constraints, directly optimizing the policy is more effective than indirectly approximating the joint value function.

2) *Long-Term Communication Performance Analysis*: To assess the performance of the proposed framework over long-

duration missions, Fig. 9b tracks the evolution of the long-term average system sum rate during the training phase.

The results demonstrate the clear dominance of the MAPPO algorithm, which rapidly ascends and stabilizes at a superior sum rate of approximately 65.5 bps/Hz. This performance advantage is fundamentally attributed to the centralized training mechanism: by leveraging a critic to evaluate the global state, MAPPO effectively guides UAVs to learn sophisticated cooperative strategies, thereby maximizing the global throughput rather than myopic local gains. In contrast, the IPPO algorithm, while occasionally reaching high peak rates, exhibits pronounced sawtooth-like oscillations. This instability reflects the inherent conflict in independent policy updates: lacking global information sharing, agents fail to anticipate the adaptive behaviors of others, creating a non-stationary learning environment where uncoordinated local improvements often destabilize the global objective. Furthermore, value-based decomposition methods prove less effective for this task. VDN suffers from severe performance fluctuations, indicating that its linear value decomposition assumption fails to approximate the highly non-linear relationship. Similarly, while QMIX maintains a smoother learning curve, it converges prematurely to a suboptimal plateau of approximately 62 bps/Hz. This stagnation suggests that the monotonicity constraint enforced by its mixing network restricts the model's expressiveness, preventing it from resolving the multi-constraint trajectory planning task.

3) *Performance Comparison with Heuristic Baselines*: To validate the superiority of the proposed learning-based planning strategy under varying traffic loads, Fig. 9c compares the long-term average system sum rate of MAPPO against two heuristic benchmarks (Greedy and Random) as the number of users increases from 8 to 24.

The results indicate that MAPPO consistently achieves the highest performance across all test densities. Specifically, while the Greedy algorithm attempts to maximize the instantaneous system sum rate at each time slot via exhaustive search, it is constrained by its myopic nature. By focusing solely on immediate rewards, the Greedy strategy fails to account for channel evolution and future positional advantages, often trapping UAVs in spatially sub-optimal regions where they cannot effectively serve users in subsequent steps. In contrast, MAPPO is explicitly designed to optimize the cumulative long-term return. It intelligently trades off immediate communication

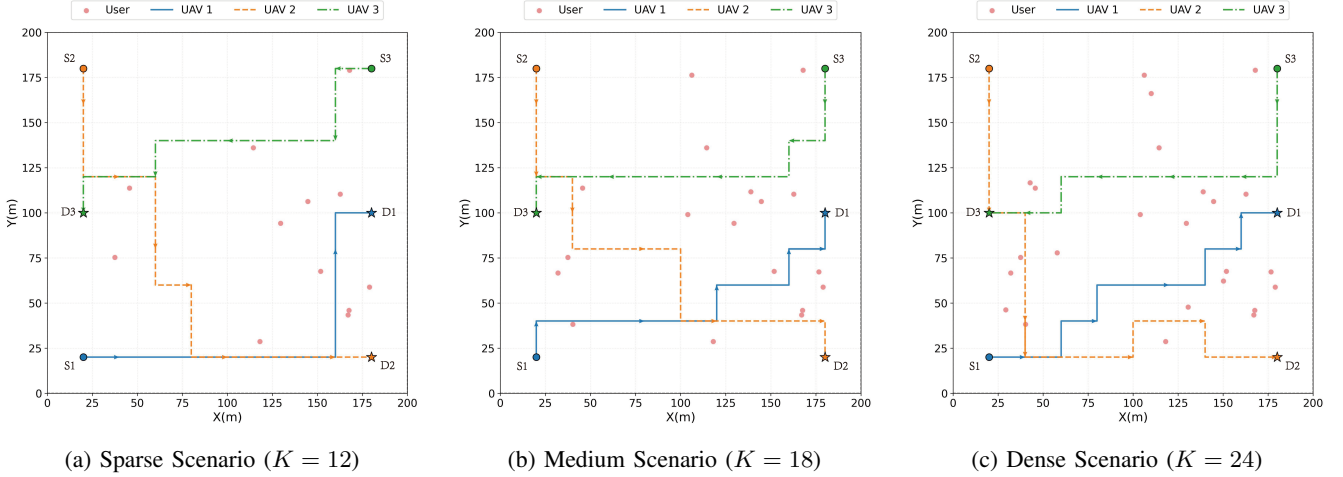


Fig. 10: Projected 2D trajectories of three UAVs navigating from start (S) to destination (D) under varying user densities.

gains for future favorable positions. For instance, strategically sacrificing a marginal rate increase in the current slot to navigate towards a region with better LoS probabilities for the remainder of the mission. This capability enables MAPPO to achieve global optimality over the entire flight duration. The Random algorithm exhibits significantly lower performance, with its slight rate increase attributed solely to passive multi-user diversity gains from higher user density rather than active trajectory management. These findings validate the critical advantage of RL in solving long-horizon, continuous-space planning tasks where instantaneous greedy decisions are often sub-optimal.

*4) Trajectory Visualization:* To visually uncover the cooperative flight strategies learned by MAPPO and assess its adaptability to dynamic environments, Fig. 10 presents the projected UAV trajectories under varying user densities: (a) Sparse, (b) Medium, and (c) Dense.

First and foremost, it is observed that in all test scenarios, every UAV successfully reaches its designated destination within the mission deadline. Notably, the generated trajectories strictly adhere to the boundary constraints without any trajectory crossing, verifying that the agents have learned robust collision avoidance capabilities via the proposed feasibility-aware reward mechanism. Furthermore, the flight paths generally follow the direction of the destinations with no redundant looping, indicating that the UAVs aim to complete the mission in near-minimal time.

Beyond basic safety and efficiency, the most distinct feature observed is service-aware maneuvering: the UAV flight paths deviate to varying degrees from the shortest straight-line path. This deviation is not random exploration but an intelligent decision driven by communication rewards, where UAVs proactively detour towards user-dense regions to shorten service distances and establish higher-quality LoS links. Crucially, this maneuvering behavior evolves significantly as the user density increases. In the sparse scenario (Fig. 10(a)), the trajectories are relatively linear, reflecting an energy-efficient strategy where the scattered users can be adequately covered without significant path deviation. However, in the dense scenario (Fig. 10(c)),

the trajectories become increasingly intricate to maximize sum-rate performance. Taking UAV 1 as a prime example: in Fig. 10(a), it follows a near-optimal straight path along the bottom edge. In stark contrast, in Fig. 10(c), UAV 1 executes a substantial upward detour towards the center of the service area. This significant lateral maneuvering enables it to provide better coverage to the dense user clusters in the bottom-middle region before proceeding to its destination. This comparison confirms that the MAPPO agents have successfully learned to dynamically trade off flight energy consumption (path length) for system sum rate maximization based on the user distribution.

## VII. CONCLUSION AND FUTURE WORK

In this paper, we proposed a hierarchically decoupled joint optimization framework for multi-UAV downlink communication networks, addressing the challenges of strong trajectory-beamforming coupling and dynamic network topologies. By decomposing the problem into two distinct timescales, we effectively integrated a topology-aware GNN for instantaneous beamforming with a MAPPO-based scheme for long-term cooperative trajectory planning. Specifically, the proposed GNN beamformer exploits the heterogeneous graph structure of user association to achieve scalable and real-time interference management. On the longer timescale, the CTDE-based MAPPO algorithm enables UAVs to learn intelligent cooperative behaviors, such as service-aware maneuvering and implicit load balancing, to maximize long-term system throughput. Extensive simulation results demonstrated that the proposed framework significantly outperforms conventional optimization heuristics and deep learning baselines in terms of sum rate performance, convergence speed, and generalization capability across varying network scales.

To enhance practical deployment, future work can extend the current discrete planning to continuous 3D control and incorporate robust designs against imperfect CSI. Furthermore, we intend to relax the orthogonal spectrum assumption to investigate full frequency reuse for higher spectral efficiency.

## REFERENCES

[1] G. Geraci et al., "What Will the Future of UAV Cellular Communications Be? A Flight From 5G to 6G," in *IEEE Communications Surveys & Tutorials*, vol. 24, no. 3, pp. 1304-1335, thirdquarter 2022, doi: 10.1109/COMST.2022.3171135.

[2] Z. Xiao et al., "Antenna Array Enabled Space/Air/Ground Communications and Networking for 6G," in *IEEE Journal on Selected Areas in Communications*, vol. 40, no. 10, pp. 2773-2804, Oct. 2022, doi: 10.1109/JSAC.2022.3196320.

[3] X. Tang et al., "Deep Graph Reinforcement Learning for UAV-Enabled Multi-User Secure Communications," in *IEEE Transactions on Mobile Computing*, vol. 24, no. 9, pp. 8780-8793, Sept. 2025, doi: 10.1109/TMC.2025.3558790.

[4] S. Wang, X. Song, T. Song and Y. Yang, "Joint Optimization of Beamforming and Trajectory for UAV-RIS-Assisted MU-MISO Systems Using GNN and SD3," in *IEEE Transactions on Mobile Computing*, vol. 24, no. 10, pp. 9539-9553, Oct. 2025, doi: 10.1109/TMC.2025.3563072.

[5] J. Chen, K. Zhai, Z. Wang, Y. Liu, J. Jia and X. Wang, "CoMP and RIS-Assisted Multicast Transmission in a Multi-UAV Communication System," in *IEEE Transactions on Communications*, vol. 72, no. 6, pp. 3602-3617, June 2024, doi: 10.1109/TCOMM.2024.3357428.

[6] S. Liu et al., "UAV-Enabled Collaborative Beamforming via Multi-Agent Deep Reinforcement Learning," in *IEEE Transactions on Mobile Computing*, vol. 23, no. 12, pp. 13015-13032, Dec. 2024, doi: 10.1109/TMC.2024.3419915.

[7] Yu, Chao, et al. "The surprising effectiveness of ppo in cooperative multi-agent games." *Advances in neural information processing systems* 35 (2022): 24611-24624.

[8] Q. Wu, Y. Zeng and R. Zhang, "Joint Trajectory and Communication Design for Multi-UAV Enabled Wireless Networks," in *IEEE Transactions on Wireless Communications*, vol. 17, no. 3, pp. 2109-2121, March 2018, doi: 10.1109/TWC.2017.2789293.

[9] Z. Xiao, H. Dong, L. Bai, D. O. Wu and X. -G. Xia, "Unmanned Aerial Vehicle Base Station (UAV-BS) Deployment With Millimeter-Wave Beamforming," in *IEEE Internet of Things Journal*, vol. 7, no. 2, pp. 1336-1349, Feb. 2020, doi: 10.1109/IJOT.2019.2954620.

[10] L. Zhu, J. Zhang, Z. Xiao, X. -G. Xia and R. Zhang, "Multi-UAV Aided Millimeter-Wave Networks: Positioning, Clustering, and Beamforming," in *IEEE Transactions on Wireless Communications*, vol. 21, no. 7, pp. 4637-4653, July 2022, doi: 10.1109/TWC.2021.3131580.

[11] X. Yuan, H. Jiang, Y. Hu and A. Schmeink, "Joint Analog Beamforming and Trajectory Planning for Energy-Efficient UAV-Enabled Nonlinear Wireless Power Transfer," in *IEEE Journal on Selected Areas in Communications*, vol. 40, no. 10, pp. 2914-2929, Oct. 2022, doi: 10.1109/JSAC.2022.3196108.

[12] S. Li, B. Duo, X. Yuan, Y. -C. Liang and M. Di Renzo, "Reconfigurable Intelligent Surface Assisted UAV Communication: Joint Trajectory Design and Passive Beamforming," in *IEEE Wireless Communications Letters*, vol. 9, no. 5, pp. 716-720, May 2020, doi: 10.1109/LWC.2020.2966705.

[13] L. Ge, P. Dong, H. Zhang, J. -B. Wang and X. You, "Joint Beamforming and Trajectory Optimization for Intelligent Reflecting Surfaces-Assisted UAV Communications," in *IEEE Access*, vol. 8, pp. 78702-78712, 2020, doi: 10.1109/ACCESS.2020.2990166.

[14] X. Pang, N. Zhao, J. Tang, C. Wu, D. Niyato and K. -K. Wong, "IRS-Assisted Secure UAV Transmission via Joint Trajectory and Beamforming Design," in *IEEE Transactions on Communications*, vol. 70, no. 2, pp. 1140-1152, Feb. 2022, doi: 10.1109/TCOMM.2021.3136563.

[15] Z. Lyu et al., "Joint maneuver and beamforming design for UAV-enabled integrated sensing and communication," *IEEE Transactions on Wireless Communications*, vol. 22, no. 4, pp. 2424-2439, Apr. 2023.

[16] G. Cheng, X. Song, Z. Lyu and J. Xu, "Networked ISAC for Low-Altitude Economy: Coordinated Transmit Beamforming and UAV Trajectory Design," in *IEEE Transactions on Communications*, vol. 73, no. 8, pp. 5832-5847, Aug. 2025, doi: 10.1109/TCOMM.2025.3541027.

[17] B. Li, H. Zhang, Y. Rong and Z. Han, "A Control-based Design of Beamforming and Trajectory for UAV-Enabled ISAC System," in *IEEE Transactions on Wireless Communications*, doi: 10.1109/TWC.2025.3604344.

[18] D. Deng, W. Zhou, X. Li, D. B. da Costa, D. W. K. Ng and A. Nallanathan, "Joint Beamforming and UAV Trajectory Optimization for Covert Communications in ISAC Networks," in *IEEE Transactions on Wireless Communications*, vol. 24, no. 2, pp. 1016-1030, Feb. 2025, doi: 10.1109/TWC.2024.3503726.

[19] J. Yu et al., "Joint 3D Beamforming-and-Trajectory Design for UAV-Satellite Uplink Covert Communication," in *IEEE Transactions on Communications*, vol. 73, no. 5, pp. 3469-3481, May 2025, doi: 10.1109/TCOMM.2024.3480979.

[20] Y. Yao et al., "UAV-Relay-Aided Secure Maritime Networks Coexisting with Satellite Networks: Robust Beamforming and Trajectory Optimization," in *IEEE Transactions on Wireless Communications*, doi: 10.1109/TWC.2025.3596136.

[21] X. Liu, Y. Liu and Y. Chen, "Machine Learning Empowered Trajectory and Passive Beamforming Design in UAV-RIS Wireless Networks," in *IEEE Journal on Selected Areas in Communications*, vol. 39, no. 7, pp. 2042-2055, July 2021, doi: 10.1109/JSAC.2020.3041401.

[22] L. Wang, K. Wang, C. Pan and N. Aslam, "Joint Trajectory and Passive Beamforming Design for Intelligent Reflecting Surface-Aided UAV Communications: A Deep Reinforcement Learning Approach," in *IEEE Transactions on Mobile Computing*, vol. 22, no. 11, pp. 6543-6553, 1 Nov. 2023, doi: 10.1109/TMC.2022.3200998.

[23] C. Liu, W. Yuan, Z. Wei, X. Liu and D. W. K. Ng, "Location-Aware Predictive Beamforming for UAV Communications: A Deep Learning Approach," in *IEEE Wireless Communications Letters*, vol. 10, no. 3, pp. 668-672, March 2021, doi: 10.1109/LWC.2020.3045150.

[24] H. -L. Chiang, K. -C. Chen, W. Rave, M. Khalili Marandi and G. Fettweis, "Machine-Learning Beam Tracking and Weight Optimization for mmWave Multi-UAV Links," in *IEEE Transactions on Wireless Communications*, vol. 20, no. 8, pp. 5481-5494, Aug. 2021, doi: 10.1109/TWC.2021.3068206.

[25] K. Guo, M. Wu, X. Li, H. Song and N. Kumar, "Deep Reinforcement Learning and NOMA-Based Multi-Objective RIS-Assisted IS-UAV-TNs: Trajectory Optimization and Beamforming Design," in *IEEE Transactions on Intelligent Transportation Systems*, vol. 24, no. 9, pp. 10197-10210, Sept. 2023, doi: 10.1109/TITS.2023.3267607.

[26] K. Guo, M. Wu, X. Li, Z. Lin and T. A. Tsiftsis, "Joint Trajectory and Beamforming Optimization for Federated DRL-Aided Space-Aerial-Terrestrial Relay Networks With RIS and RSMA," in *IEEE Transactions on Wireless Communications*, vol. 23, no. 12, pp. 18456-18471, Dec. 2024, doi: 10.1109/TWC.2024.3468298.

[27] B. Yin, X. Fang, X. Wang, L. Yan, J. Wu and J. Wang, "Trajectory Design and Beamforming in UAV-Assisted Wireless Networks: A Fine-Tuned M2LLM-Driven DRL-Based Framework," in *IEEE Transactions on Wireless Communications*, doi: 10.1109/TWC.2025.3605277.

[28] P. Li et al., "Graph neural network-based scheduling for multi-UAV-enabled communications in D2D networks," *Digital Communications and Networks*, vol. 10, no. 1, pp. 45-52, 2024.

[29] H. Zhao, K. Liu, M. Liu, S. Garg and M. Alrashoud, "Intelligent Beamforming for UAV-Assisted IIoT Based on Hypergraph Inspired Explainable Deep Learning," in *IEEE Transactions on Consumer Electronics*, vol. 70, no. 1, pp. 1972-1982, Feb. 2024, doi: 10.1109/TCE.2023.3325128.

[30] Q. Wang, Y. Lu, W. Chen, B. Ai, Z. Zhong and D. Niyato, "GNN-Enabled Optimization of Placement and Transmission Design for UAV Communications," in *IEEE Transactions on Vehicular Technology*, vol. 74, no. 4, pp. 6656-6661, April 2025, doi: 10.1109/TVT.2024.3514860.

[31] Y. Pan, X. Wang, Z. Xu, N. Cheng, W. Xu and J. -J. Zhang, "GNN-Empowered Effective Partial Observation MARL Method for AoI Management in Multi-UAV Network," in *IEEE Internet of Things Journal*, vol. 11, no. 21, pp. 34541-34553, 1 Nov. 2024, doi: 10.1109/IJOT.2024.3447774.

[32] Z. Chen, Z. Zhang, Z. Xiao, Z. Yang and R. Jin, "Deep Learning-Based Multi-User Positioning in Wireless FDMA Cellular Networks," in *IEEE Journal on Selected Areas in Communications*, vol. 41, no. 12, pp. 3848-3862, Dec. 2023, doi: 10.1109/JSAC.2023.3322799.

[33] M. Mozaffari, W. Saad, M. Bennis and M. Debbah, "Efficient Deployment of Multiple Unmanned Aerial Vehicles for Optimal Wireless Coverage," in *IEEE Communications Letters*, vol. 20, no. 8, pp. 1647-1650, Aug. 2016, doi: 10.1109/LCOMM.2016.2578312.

[34] T. Cai, S. Luo, K. Xu, D. He, T.-Y. Liu, and L. Wang, "GraphNorm: A principled approach to accelerating graph neural network training," in *Proc. Int. Conf. Mach. Learn. (ICML)*, Jul. 2021, pp. 1204-1215.

[35] S. Katoch, S. S. Chauhan, and V. Kumar, "A review on Genetic Algorithm: Past, present, and future," *Multimedia Tools and Applications*, vol. 80, no. 5, pp. 8091-8126, Oct. 2020. doi:10.1007/s11042-020-10139-6

[36] J. Blank and K. Deb, "Pymoo: Multi-Objective Optimization in Python," in *IEEE Access*, vol. 8, pp. 89497-89509, 2020, doi: 10.1109/ACCESS.2020.2990567.

[37] M. Zaheer, S. Kottur, S. Ravvanbakhsh, B. Poczos, R. Salakhutdinov, and A. Smola, "Deep sets," *arXiv preprint arXiv:1703.06114*, 2018.

[38] C. R. Qi, L. Yi, H. Su, and L. J. Guibas, "PointNet++: Deep hierarchical feature learning on point sets in a metric space," in *Proc. Adv. Neural Inf. Process. Syst. (NIPS)*, Long Beach, CA, USA, Dec. 2017, pp. 5099-5108.

[39] P. Sunehag et al., "Value-decomposition networks for cooperative multi-agent learning," in *Proc. Int. Conf. Auto. Agents Multiagent Syst. (AAMAS)*, Stockholm, Sweden, Jul. 2018, pp. 2085-2087.

[40] T. Rashid, M. Samvelyan, C. S. De Witt, G. Farquhar, J. Foerster, and S. Whiteson, “Monotonic value function factorisation for deep multi-agent reinforcement learning,” *J. Mach. Learn. Res.*, vol. 21, no. 178, pp. 1–51, 2020.